ANALYSIS OF CHARACTERISTICS OF TWO CLOSE STATIONARY HUMAN TARGETS DETECTED BY IMPULSE RADIO UWB RADAR

Y. F. Li, X. J. Jing, H. Lv, and J. Q. Wang*

School of Biomedical Engineering, The Fourth Military Medical University, Xi'an, Shaanxi 710032, China

Abstract—The detection and identification of multi-stationary human targets with IR-UWB radar is a new and important technology. This paper is focused on the detection and identification of two close stationary human targets by using monostatic IR-UWB radar with low center frequency. For this purpose, the characteristics of the radar echoes from two close stationary human targets are processed and analyzed. Furthermore, the effect that the interference behind the anterior target affects the signal of posterior target is represented, and the features of this interference are interpreted. According to the analyses, a method using adaptive cancellation is proposed to attenuate the interference and improve the detection and identification of two close stationary human targets. Series of experiments are done in different scenarios, and the results of the experiments are presented to demonstrate the validity of the method. It has been shown that the proposed method can attenuate the interference and make the detection and identification of multi-human targets more precise.

1. INTRODUCTION

Ultra-wide band (UWB) is a widely used technology in clinical medicine, rescue missions, surveillance and anti-terrorism [1–5]. As a type of UWB technology, Impulse Radio (IR) UWB plays an important role in the detection of human targets [6–10], especially in the scenes of penetrating obstacles, such as walls, snow and rubbles [11–15]. Therefore, researches of life detection based on IR-UWB radar are widely developed. IR-UWB radar can detect human targets mainly based on the motion or the respiration of humans. Consequently,

some researches aim at tracking moving human targets [14, 16], and some researches aim at the detection and identification of stationary human targets [2, 17, 18]. With the development in the detection of stationary human targets, many researches are focused on the detection and identification of multi-stationary human targets. Most of these researches require targets keeping considerable distance from each other, and the distance is usually more than 1 m [17]. However, the distance is probably less than 1 m in practical situation, so there are still some researches focused on this situation. For example in [2], the radial distance between targets is about 0.6 m, and the minimum angle between the azimuths of the targets is 14°. These researches usually take advantage of the radar systems with high center frequency. For example, the center frequency of the radar involved in [2] is higher than 3 GHz. It is just the high center frequency that provides high spatial resolution. The disadvantage of using high center frequency is that it usually makes the penetration ability of the radar systems weak. Moreover, in the practical applications, such as post-earthquake rescue, the penetration ability must be taken into account. Therefore, the detection in such kind of applications should focus on the IR-UWB radar with low center frequency. However, the detection of close targets by radar with low center frequency has not been well solved, because the characteristics of signals in this situation are not well known.

Previous experiments by using the radar with low center frequency have shown that in the situation with close stationary human targets, the target located the most closely to the radar is often easy to be detected. The rest targets can also be detected but with less reliability. This effect, to a large extent, lowers the efficiency of the radar performance in detection of multi-stationary human targets.

The aim of the paper is to analyze this effect and find a method to eliminate the effect so as to improve the radar performance efficiency in detection of multi-stationary human targets. In order to achieve this aim, a monostatic IR-UWB radar with low centre frequency is implemented to perform detection. Furthermore, the characteristics of the signals are analyzed. The result shows that as the two targets are relatively close, interference behind the anterior target would affect the signal of the posterior target. Because of the interference, it is difficult to distinguish the signals in this kind of scenario from the signals in the scenario with only one stationary human target. Therefore, the adaptive cancellation is proposed to suppress the interference in order to have better identification of the multi-stationary human targets.

The rest of this paper is organized as follows. Section 2 presents and discusses the proposed measurement setup. The signal pre-processing and analyses are described in Section 3. The adaptive
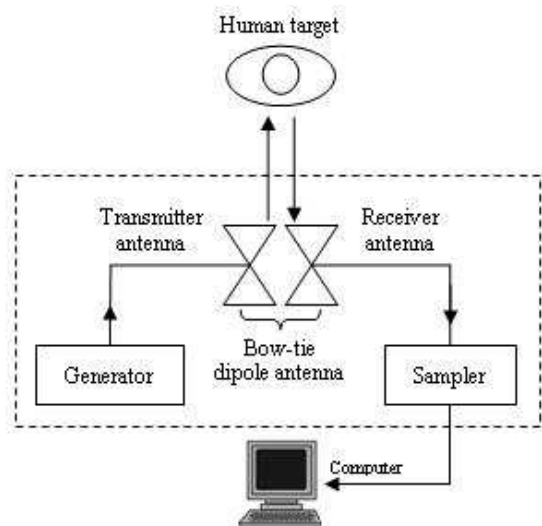
Figure 1. Monostatic IR-UWB radar setup.

cancellation applied to the pre-processed data is presented in Section 4. Results from different experiments are presented and discussed in Section 5. Conclusions are drawn in Section 6.

2. UWB SYSTEM

The monostatic IR-UWB radar setup is shown in Figure 1. The pulse generator produces pulses with a pulse repetition frequency (PRF) of 128 kHz. The pulses are sent to the transmitter and shaped into bipolar pulses to excite the bow-tie dipole antenna. The vertically polarized pulses are transmitted with a peak power of about 5 W.

The reflected pulses are received by the receiver antenna which is identical to the transmitter antenna. The shape and the spectrum of the received pulse are shown in Figure 2. As the figure shows, the center frequency and the bandwidth of the received pulse are both 400 MHz. In addition, the received pulses are range-gated, amplified and integrated in sampler, then stored in form of waveforms. The waveforms are sampled by using 8192 points and the recorded duration is 80 ns. The time-axis along each received waveform is addressed as "fast-time", and is in the order of nanoseconds. The interval between successive received waveforms is $T_s = 0.0625$ s. The time-axis along the interval is termed as "slow-time", and is in the order of seconds. Accordingly, the sampling frequency in slow-time is $F_s = \frac{1}{T_s} = 16$ Hz,
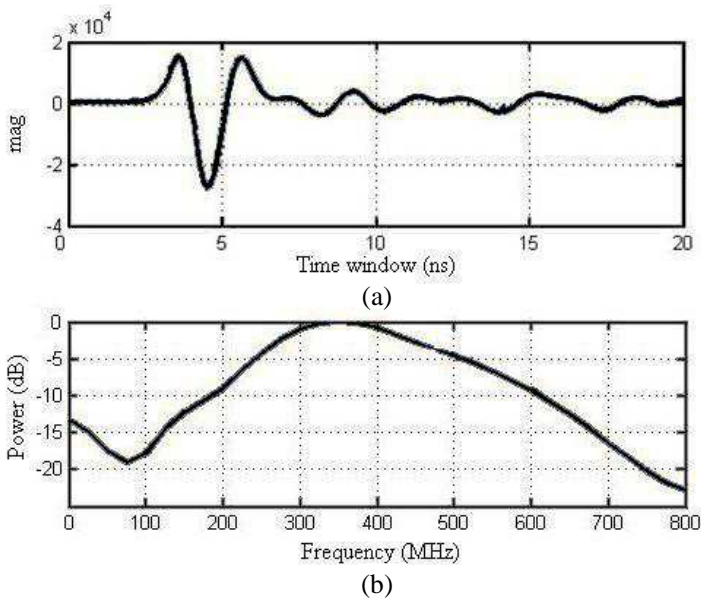
Figure 2. (a) The shape of the received pulse and (b) the spectrum of the received pulse.

which is greater than the Nyquist sampling rate for the heart and respiration signals. The length of recorded data is about 60 s.

3. SIGNAL PROCESSING AND ANALYSES

In this section, the phenomenon mentioned in Section 1 will be analyzed. For this purpose, a mathematical model is developed so that the signal processing and analysis can be better interpreted and understood. As mentioned in Section 2, the received waveforms are measured at discrete instants in slow-time $t = nT_s$ $(n = 1, 2, \ldots, N)$, and the discrete-time sequences are sampled in every sampling period in fast-time $\tau = mT_f$ $(m = 1, 2, \ldots, M)$. These values are stored in a $(N \times M)$ matrix $\mathbf{R}$.

According to [12], there are large amounts of clutters and noise in the acquired data, so some pre-processing methods need to be applied to the data to remove them before signal analysis. First, a smoothing filter, which is a low pass filter, is applied in each waveform to deal with the presence of substantial random noise, especially the Additive White Gaussian Noise (AWGN). Second, in order to remove the background clutters caused by stationary objects, the average of all waveforms
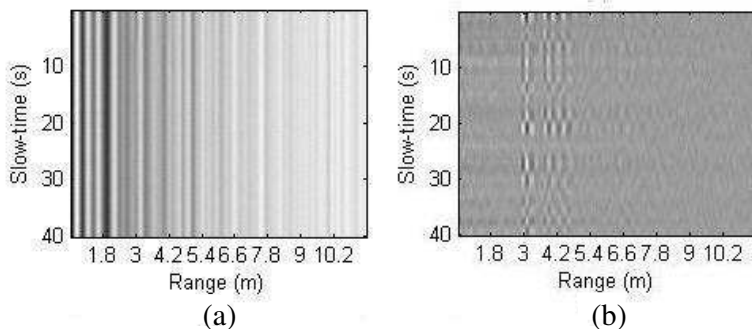
Figure 3. (a) Data received from the scenario depicted in Figure 1, and (b) data after pre-processing.

(rows) is subtracted from each waveform. Finally, a Finite Impulse Response (FIR) filter is accomplished to suppress the high frequency noise in slow-time dimension. After these steps, the new matrix is represented by **W**, and the matrix **W** can be expressed as follows:

$$\mathbf{W} = (w_1, w_2, \ldots, w_M) \tag{1}$$

where w_i is the vector along the slow-time dimension, and m is the index in the fast-time dimension.

Figure 3 shows the raw data and the data after pre-processing. As the figure shows, the regular fluctuation can be seen directly after all the steps. The fluctuation in Figure 3(b) is aroused by the respiration of the human target. In order to identify the target, the power spectrum of the pre-processed data is given by calculating variances along the slow-time, and depicted in Figure 4(a). The magnitude of the respiration component in the power spectrum is large, so the location of the target can be estimated by finding the maximum peak in the power spectrum. The signal at the peak can be represented by vector w_τ.

Figure 4(a) is the power spectrum of the data from the scenario depicted in Figure 1. The magnitude represents the power of the signals in different range. The larger and more regular the signal along slow-time dimension is, the larger its magnitude in power spectrum becomes. As mentioned above, the respiration signal is regular and large in the pre-processed data. As a result, the magnitude of the power spectrum in the range where the target locates is large. The power around 1 m is chosen to be a threshold to identify human target. Because the magnitude of the maximum peak of the power spectrum
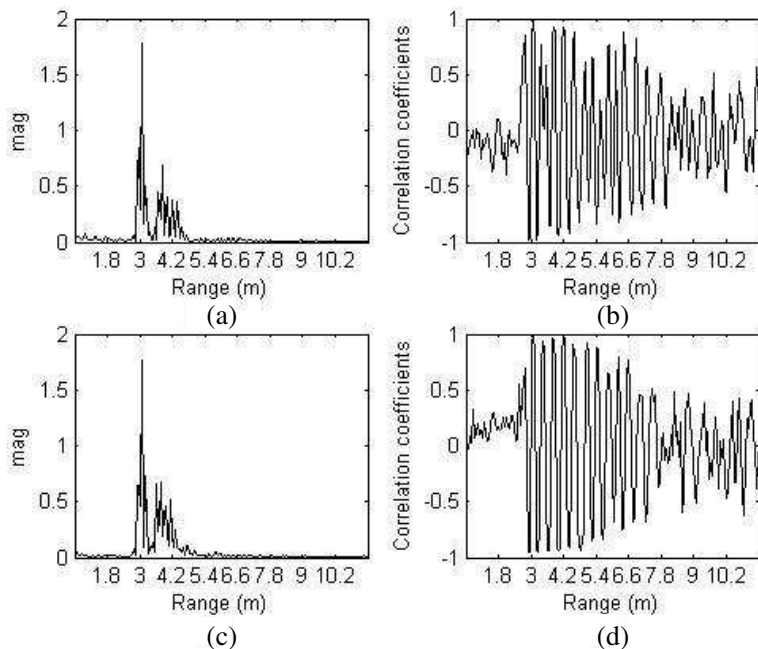
Figure 4. (a) The power spectrum of the data from the scenario depicted in Figure 1, (b) the correlation coefficients in Figure 1, (c) the power spectrum of the pre-processed data acquired in the scenario with two close stationary human targets, and (d) the correlation coefficients in the scenario with two stationary human targets.

is much higher than the threshold, the human target can be decided. The maximum peak corresponds to the location of the target. As Figure 4(a) shows, not only the magnitude of the power spectrum in the range where the target locates is large, but the magnitude behind the target is large as well. In order to analyze the relationship of vectors along slow-time dimension in different ranges, the correlation coefficients between w_τ and w_i $(i = 1, 2, \ldots, N)$ have been calculated, and shown in Figure 4(b). As the figure shows, the correlation between the target signal and signals behind the target is rather high.

In order to analyze the situation of the detection of multi-stationary human targets, detections of two stationary human targets by using the same IR-UWB radar with low center frequency in the same environment have also been performed. After pre-processing, the power spectrum of the data acquired in this scenario has been

calculated and drawn in Figure 4(c). The signal along slow-time dimension at the maximum peak of the power spectrum corresponds to the anterior target signal, and represented by vector w_τ. The correlation coefficients between w_τ and w_i $(i = 1, 2, \ldots, N)$ have been calculated and shown in Figure 4(d). In Figure 4(c), the magnitude of the power spectrum is large in the range where the anterior target locates, and the magnitude in the range where the posterior target locates is much lower than the one of the anterior target. In Figure 4(d), the correlation between the anterior target signal and signals behind the target is high. As the figure shows, the shape of the power spectrum in Figure 4(c) just looks like the one in Figure 4(a), and the correlation coefficients in Figures 4(d) and 4(b) also are similar with each other.

Analyses above show that respiration of a target interferes with the signals behind the target. The interference is represented as the large magnitude in the power spectrum and the high correlation with the signal of the target. Because of the interference, figures of power spectrums and correlation coefficients from situations mentioned above are similar. Therefore, it is difficult to identify the number of human targets.

4. ADAPTIVE CANCELLATION

In order to identify the number of human targets, the interference needs to be attenuated. The traditional method for this purpose is the fixed notch filter [20–24] which needs to be tuned to the frequency of the interference. Especially in the two close targets scenario, the frequencies of different human respiration signals are really close, so the notch is required to be very sharp. Besides, the precise frequency of the interference is necessary for the filter designing. However, because the
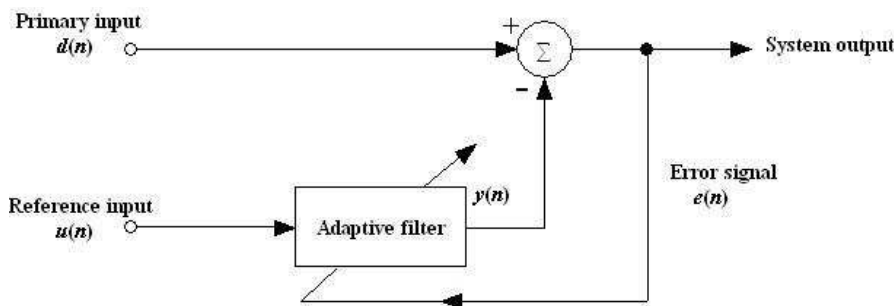

Figure 5. The block diagram of adaptive cancellation.

human respiration signals drift slowly with time, the precise frequency of respiration signals is hard to acquire. As the traditional method can not be used to satisfy all the needs, what is needed in this situation is a method which can adjust its parameters automatically according to the interference.

From the correlation analysis, it can be concluded that signal of target and the interference behind it are correlated in a certain extent. As a result, the signal of target can be considered as the reference of the interference. Moreover, the interference is assumed to be additive. Therefore, the adaptive cancellation would perform well to attenuate the interference.

The adaptive cancellation is one configuration of the adaptive filter which performs satisfactorily in an environment where complete knowledge of the relevant signal characteristics is not available [19]. Figure 5 shows the block diagram of adaptive cancellation. The primary input contains the signal which is concerned about and the interference.

$$d(n) = s(n) + A_0 i(n) \qquad (2)$$

where $d(n)$ is the primary input, $s(n)$ is the concerned signal, A_0 is the amplitude of the interference, and $i(n)$ is the normalized interference. Moreover, the reference input supplies a correlative version of the
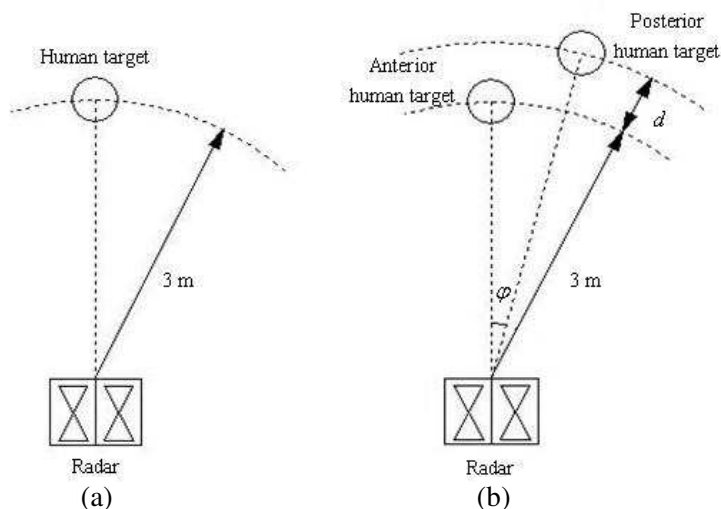

Figure 6. Scenarios for unobstructed case. (a) Scenario with single target and (b) scenario with two close targets.

interference.

$$u(n) = Ai(n) \tag{3}$$

where $u(n)$ is the reference input, and $i(n)$ is the normalized interference with different amplitude A. The reference input of the adaptive cancellation provides an estimation of the interference contained in the primary input. Therefore, the effect of the interference can be attenuated by subtracting the adaptive filter output from the primary input. For the adaptive filter, the tap weights of the filter are adapted by means of the Least-Mean-Square (LMS) algorithm.

$$y(n) = \sum_{i=0}^{L-1} \hat{\omega}_i(n)u(n-i) \tag{4}$$

$$e(n) = d(n) - y(n) \tag{5}$$

$$\hat{\omega}_i(n+1) = \hat{\omega}_i(n) + \mu u(n-i)e(n), \quad i = 0, 1, \ldots, L-1 \tag{6}$$

where L is the order of the filter, μ is the step-size parameter, and $\hat{\omega}_i(n)$ is the tap weight.
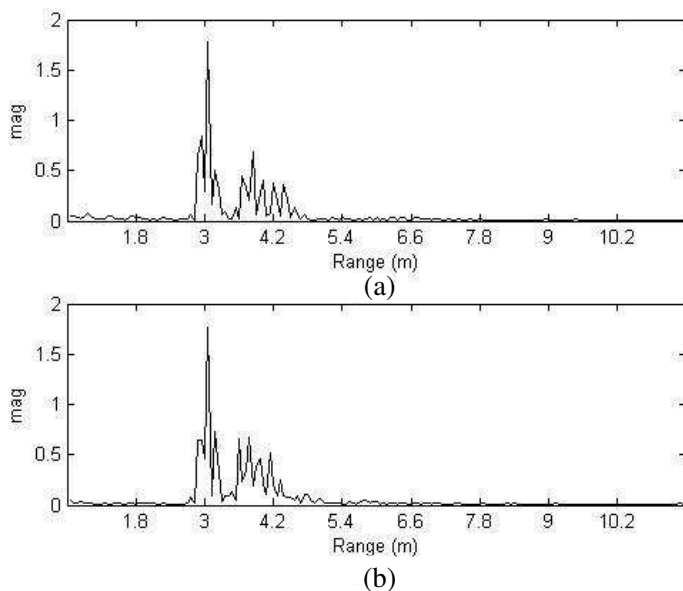

Figure 7. (a) Power spectrum of the data from the first scenario in no obstacle case, and (b) power spectrum of the data from the second scenario in no obstacle case.

In this paper, the primary input is the signal behind a target. The reference input is the signal of the target. By attenuating the interference from the signals behind the target, the respiration signal of the other target will be only left in the scenario of two targets, whereas there will be no respiration signal left in the scenario of single target.

5. EXPERIMENTAL RESULTS

In this section some experimental results are presented. Two cases are considered: (1) No obstacle is between targets and antennas. (2) A 24 cm thick brick wall is between targets and antennas.

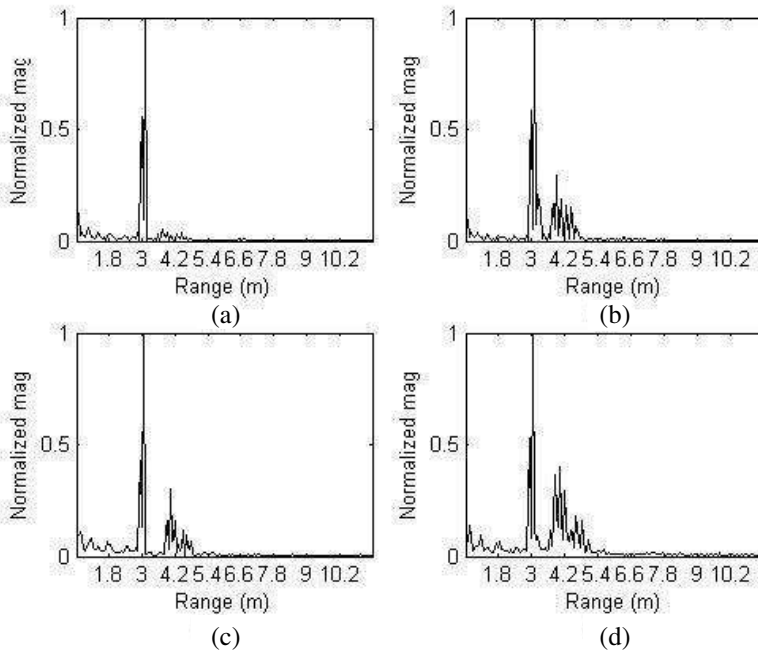In the first case, experiments were accomplished in scenarios which

Figure 8. Power spectrums in unobstructed case. (a) The power spectrum of the data after adaptive cancellation in the first scenario, (b) the power spectrum of the data after notch filter in the first scenario, (c) the power spectrum of the data after adaptive cancellation in the second scenario, and (d) the power spectrum of the data after notch filter in the second scenario.

can be illustrated by Figure 6. As Figure 6(a) shows, the first scenario is only one human target keeping stationary located 3 m away from the antennas. The measured data have been pre-processed, and then the power spectrum has been calculated and presented in Figure 7(a). The second scenario is the same person keeping stationary located at the same distance (3 m away from the radar) with another human target keeping stationary located 1 m behind the first person. This

Table 1. Some other scenarios for the unobstructed case.

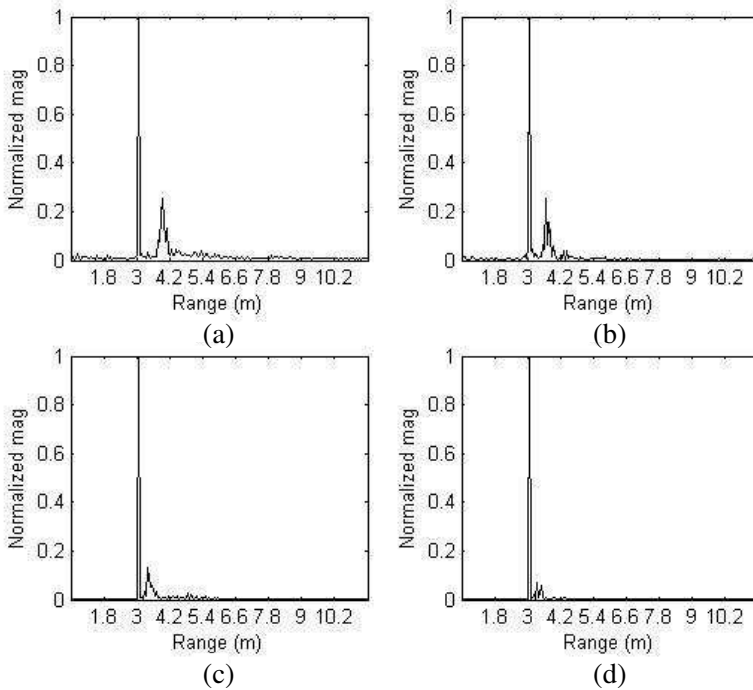| Scenarios	Value of φ and d
(a)	$\varphi = 10°$, $d = 0.8\,\text{m}$
(b)	$\varphi = 10°$, $d = 0.6\,\text{m}$
(c)	$\varphi = 10°$, $d = 0.4\,\text{m}$
(d)	$\varphi = 10°$, $d = 0.2\,\text{m}$

Figure 9. Scenarios for the unobstructed case depicted in Table 1.

scenario can be illustrated by Figure 6(b). In Figure 6(b), φ denotes
the angle between the azimuths of two targets, and is equal to $10°$. d
represents the difference between the radial distances of two targets.
In this scenario, d is equal to $1\,m$ which means the radial distance of
the second target is $4\,m$. Figure 7(b) shows the power spectrum of
the pre-processed data of the second scenario. From Figure 7, it can
be seen that the situation discussed in Section 3 has been proved. In
these two scenarios, the power spectrums are almost the same. By
finding the maximum peak in the power spectrums, one target can
be determined in both scenarios. The detected locations in the two
scenarios are both $3.06\,m$. The magnitude of the power spectrums
behind the determined targets in two scenarios is obvious, and has
little difference. It is difficult to distinguish between the two scenarios
according to these two figures.

Then both the adaptive cancellation and the notch filter have been
applied to the data acquired in these two scenarios. The normalized
power spectrums of the data after each method have been calculated
and shown in Figure 8. Data acquired in the first scenario are processed
by the adaptive cancellation, and the power spectrum of the data is
depicted in Figure 8(a). As the figure shows, there is no obvious peak in
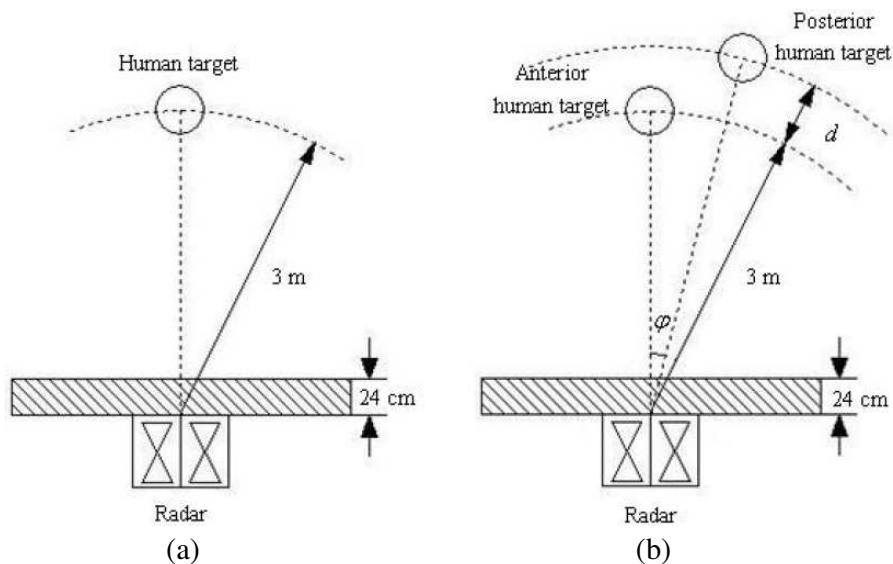the power spectrum behind the determined target after the adaptive

Figure 10. Scenarios for obstructed case. (a) Scenario with single
target and (b) scenario with two close targets.

cancellation. Then, it can be decided that there is only one target in the detection area. Data acquired in the second scenario are also processed by using the adaptive cancellation, and the power spectrum is depicted in Figure 8(c). As the figure shows, there is an obvious peak in the power spectrum behind the determined target, but this peak is lower than the maximum one. Still, it is easy to decide there is another target in the detection area. This lower peak corresponds to the location of the posterior target, and the detected location of the posterior target is 4.02 m. Data from the two scenarios are also processed by notch filter, and their power spectrums are depicted in Figures 8(b) and 8(d). As figures show, the magnitude in the range behind the determined target becomes lower in both figures, but still significant. It is hard to tell the difference between these two figures, so it can not distinguish between the two scenarios directly.

Further experiments are done in some other scenarios which are illustrated by Figure 6(b). In these scenarios, φ is still equal to 10°, and d in each scenario is listed in Table 1. The data acquired from these scenarios are processed by adaptive cancellation, and the power
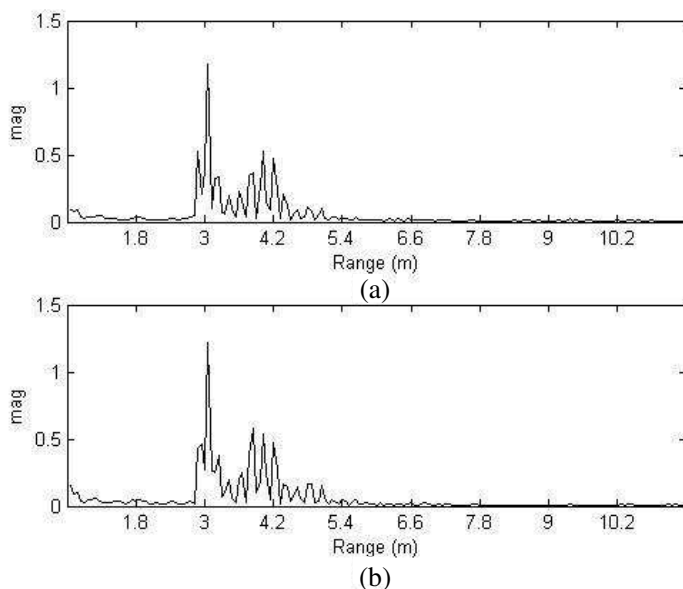

Figure 11. (a) Power spectrum of the data from the first scenario in obstacle case, and (b) power spectrum of the data from the second scenario it in obstacle case.

spectrums of the processed data are depicted in Figure 9. The figures show that as the distance of two targets becomes smaller, the power of the second target becomes weaker. However, only one target can be decided from the Figure 9(d) when $d = 0.2$ m.

In the second case, a 24 cm thick brick wall is in front of the radar. The antennas were laid against the brick wall, and the targets locate towards to the antennas on the other side of the wall. The experiments are also done in some scenarios in this case. Except the brick wall, these scenarios are as same as the ones in the first case. Scenarios in this case can be illustrated by Figure 10. Figure 11 shows the power spectrums of the pre-processed data of the first two scenarios. Although the magnitude of the power spectrums is low in both scenarios, one target still can be determined by finding the
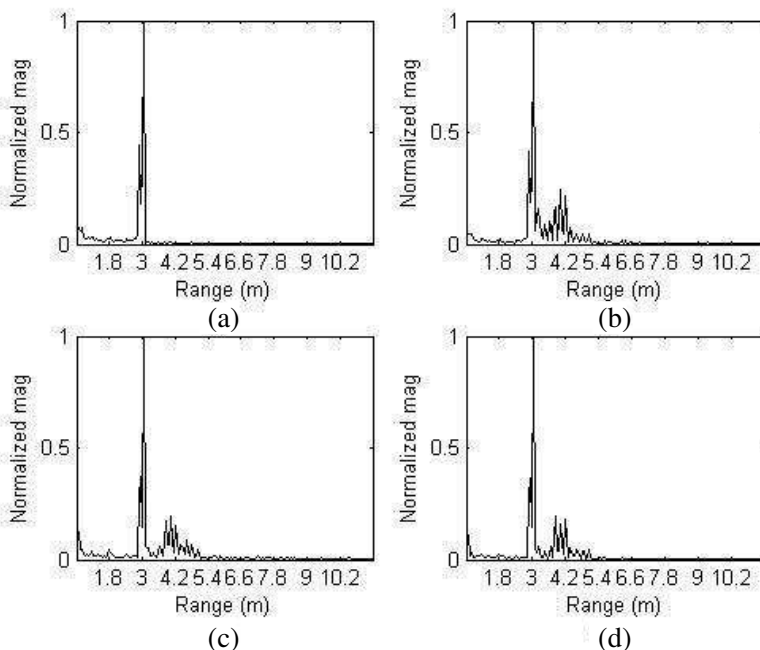

Figure 12. Power spectrums in obstructed case. (a) The power spectrum of the data acquired in the first scenario after adaptive cancellation, (b) the power spectrum of the data acquired in the first scenario after notch filter, (c) the power spectrum of the data acquired in the second scenario after adaptive cancellation, and (d) the power spectrum of the data acquired in the second scenario after notch filter.

Table 2. Some other scenarios for the obstructed case.

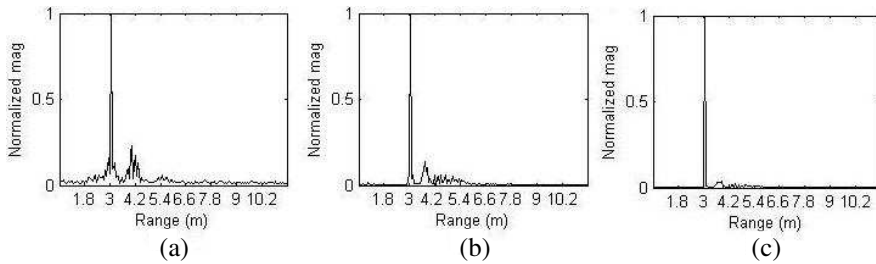| Scenarios	Value of φ and d
(a)	$\varphi = 10°$, $d = 0.8\,\mathrm{m}$
(b)	$\varphi = 10°$, $d = 0.6\,\mathrm{m}$
(c)	$\varphi = 10°$, $d = 0.4\,\mathrm{m}$

Figure 13. Scenarios for the obstructed case depicted in Table 2.

maximum peak in each power spectrum. The detected locations in these two scenarios are both 3.06 m. The adaptive cancellation and the notch filter have been applied to the data in both scenarios, and the normalized power spectrums of the data after processing are shown in Figure 12. As Figure 12 shows, it can be decided that there is only one target in the first scenario, and there are two targets in the second scenario. The detected location of the posterior target in the second scenario in this case is 4.02 m. This result is same as the result in no obstacle case. Experiments are still done in some other scenarios which can be illustrated by Figure 10(b). In these scenarios, φ is equal to $10°$, and d is listed in Table 2. The power spectrums of the data processed by adaptive cancellation in these scenarios are shown in Figure 13. As the figures show, the closer the two targets are, the weaker the power of the second target is. Only one target can be decided from Figure 13(c) when $d = 0.4\,\mathrm{m}$.

6. CONCLUSION

In this paper, the study on the detection and identification of two close stationary human targets by using monostatic IR-UWB radar with low center frequency has been presented. The power spectrums and the correlations of the signals acquired by the radar system in different scenarios have been analyzed. The analyses show that the signals of

the target affect the signals behind the target. This effect acts as interference in the detection and identification of two close stationary human targets. Because of the interference, it is difficult to distinguish the power spectrums of the data in the scenarios of one single human target from those in the scenarios of two close human targets. The interference also makes the signals in the range where the posterior target locates highly correlated to the signals of the anterior target. Both the two features make it difficult to detect and identify two close stationary human targets precisely. Considering all the characteristics of the interference, the adaptive cancellation has been proposed to attenuate the interference.

Experiments have been done in both obstructed and unobstructed cases, and each case includes some scenarios. Both adaptive cancellation and notch filter have been applied to the data acquired from the first two scenarios. As the results show, after the adaptive cancellation, the spectrum from the scenario of single target has only one peak, whereas the spectrum from the scenario of two close targets has two peaks. It is easy to distinguish one scenario from another. However, after the notch filter, all the spectrums from these two scenarios have two peaks. It is still difficult to distinguish the scenarios and decide the precise number of the targets. Besides, the experiments in the obstructed case show that the adaptive cancellation can still work well in penetration conditions.

Some other experiments are done in the scenario with the difference of the radial distances between two targets under 1 m. As the results show, the power of the posterior target in the power spectrum becomes lower when the difference is getting smaller. However, only one target can be identified after adaptive cancellation when the difference is too small, and the minimum difference in obstructed case is smaller than the one in unobstructed case. This is because the identification capability of IR-UWB radar may be associated with its spatial resolution, which becomes low after penetrating through the brick wall. In order to solve this problem, bistatic and multistatic radar systems should be considered, which can increase the radial distances between two targets by properly allocating the transmitter and receiver antennas. Furthermore, the research in this paper can provide help for human detection with these systems. Meanwhile, the research in this paper can improve the detection and identification of the multi-stationary human targets as well. As a result, this improvement in the performance of the radar system can make the system meet the requirement of practical application.

REFERENCES

1. Lazaro, A., D. Girbau, and R. Villarino, "Analysis of vital signs monitoring using an IR-UWB radar," *Progress In Electromagnetics Research*, Vol. 100, 265–284, 2010.

2. Rivera, N. V., S. Venkatesh, C. Anderson, and R. M. Buehrer, "Multi-target estimation of heart and respiration rates using ultra wideband sensors," *14th European Signal Processing Conference*, 4–9, 2006.

3. Lazaro, A., D. Girbau, and R. Villarino, "Simulated and experimental investigation of microwave imaging using UWB," *Progress In Electromagnetics Research*, Vol. 94, 263–280, 2009.

4. AlShehri, S. A., S. Khatun, A. B. Jantan, R. S. A. Raja Abdullah, R. Mahmood, and Z. Awang, "3D experimental detection and discrimination of malignant and benign breast tumor using NN-based UWB imaging system," *Progress In Electromagnetics Research*, Vol. 116, 221–237, 2011.

5. McGinley, B., M. O'Halloran, R. C. Conceição, G. Higgins, E. Jones, and M. Glavin, "The effects of compression on ultra wideband radar signals," *Progress In Electromagnetics Research*, Vol. 117, 51–65, 2011.

6. Shaban, H. A., M. A. El-Nasr, and R. M. Buehrer, "Localization with sub-millimeter accuracy for UWB-based wearable human movement radar systems," *Journal of Electromagnetic Waves and Applications*, Vol. 25, No. 11–12, 1633–1644, 2011.

7. Byrne, D., M. O'Halloran, E. Jones, and M. Glavin, "Support vector machine-based ultrawideband breast cancer detection system," *Journal of Electromagnetic Waves and Applications*, Vol. 25, No. 13, 1807–1816, 2011.

8. Bui, V. P., X.-C. Wei, and E. P. Li, "An efficient simulation technology for characterizing the ultra-wide band signal propagation in a wireless body area network," *Journal of Electromagnetic Waves and Applications*, Vol. 24, No. 17–18, 2575–2588, 2010.

9. AlSHehri, S. A., S. Khatun, A. B. Jantan, R. S. A. Raja Abdullah, R. Mahmood, and Z. Awang, "Experimental breast tumor detection using nn-based UWB imaging," *Progress In Electromagnetics Research*, Vol. 111, 447–465, 2011.

10. Conceição. R. C., M. O'Halloran, E. Jones, and M. Glavin, "Investigation of classifiers for early-stage breast cancer based on radar target signatures," *Progress In Electromagnetics Research*, Vol. 105, 295–311, 2010.

11. Crowgey. B. R., E. J. Rothwell, L. C. Kempel, and E. L. Mokole, "Comparison of UWB short-pulse and stepped-frequency radar systems for imaging through barriers," *Progress In Electromagnetics Research*, Vol. 110, 403–419, 2010.

12. Lv, H., G. H. Lu, X. J. Jing, and J. Q. Wang, "A new ultra-wideband radar for detecting survivors bured under earthquake rubbles," *Microwave and Optical Technology Letters*, Vol. 52, No. 11, 2621–2624, 2010.

13. Zhu. F., S. C. S. Gao, A. T. S. Ho, T. W. C. Brown, J. Li, and J. D. Xu, "Low-profile directional ultra-wideband antenna for see-through-wall imaging applications," *Progress In Electromagnetics Research*, Vol. 121, 121–139, 2011.

14. Nezirović, A. N., "Trapped-victim detection in post-disaster scenarios using ultra-wideband radar," Ph.D. Theses, Faculty Electrical Engineering, Mathematics and Computer Science, 2010.

15. Jia. Y., L. Kong, and X. Yang, "A novel approach to target localization through unknown walls for through-the-wall radar imaging," *Progress In Electromagnetics Research*, Vol. 119, 107–132, 2011.

16. Nag, S., M. A. Barnes, T. Tim, and W. H. Gary, "An ultra-wideband through-wall radar for detecting the motion of people in real time," *International Symposium on Laser Metrology Applied to Science, Industry, and Everyday Life*, 48–57, 2002.

17. Greneker III, E. F., "Radar sensing of heartbeat and respiration at a distance with security applications," *Proceedings of SPIE*, Vol. 3066, 22–27, 1997.

18. Chiani, M., A. Giorgetti, M. Mazzotti, R. Minutolo, and E. Paolini, "Target detection metrics and tracking for UWB radar sensor networks," *IEEE International Conference on Ultra-Wideband, 2009, ICUWB 2009*, 469–474, 2009.

19. Akiyama, I., M. Enokito, and A. Ohya, "Development of an UWB rescue radar system," *Proceedings of International Conference of Infomation Processing and Management of Uncertainty in Knowledge-Based Systems*, 2119–2126, 2006.

20. Ni, J., B. Chen, S. L. Zheng, X.-M. Zhang, X.-F. Jin, and H. Chi, "Ultra-wideband bandpass filter with notched band based on electrooptic phase modulator and phase-shift fiber Bragg grating," *Journal of Electromagnetic Waves and Applications*, Vol. 24,

No. 5–6, 795–802, 2010.

21. Wei. F., L. Chen, Q.-Y. Wu, X.-W. Shi, and C.-J. Gao, "Compact UWB bandpass filter with narrow notch-band and wide stop-band," *Journal of Electromagnetic Waves and Applications*, Vol. 24, No. 7, 911–920, 2010.

22. Xu. J., B. Li, H. Wang, C. Miao, and W. Wu, "Compact UWB bandpass filter with multiple ultra narrow notched bands," *Journal of Electromagnetic Waves and Applications*, Vol. 25, No. 7, 987–998, 2011.

23. Huang. J.-Q., Q.-X. Chu, and C.-Y. Liu, "Compact UWB filter based on surface-coupled structure with dual notched bands," *Progress In Electromagnetics Research*, Vol. 106, 311–319, 2010.

24. Hsiao. P. Y. and R. M. Weng, "Compact tri-layer ultra-wideband bandpass filter with dual notch bands," *Progress In Electromagnetics Research*, Vol. 106, 49–60, 2010.